Arrays of Densely Packed Isolated Nanowires by Focused Beam Induced Deposition Plus Ar^+ Milling

José María De Teresa[†,‡,§,*] and Rosa Córdoba[‡,§,⊥]

[†]Instituto de Ciencia de Materiales de Aragón (ICMA), Universidad de Zaragoza—CSIC, 50009 Zaragoza, Spain, [‡]Departamento de Física de la Materia Condensada, Universidad de Zaragoza, 50009 Zaragoza, Spain, and [§]Laboratorio de Microscopías Avanzadas (LMA), Instituto de Nanociencia de Aragón (INA), Universidad de Zaragoza, 50018 Zaragoza, Spain. [⊥]Present address: Department of Applied Physics, Eindhoven University of Technology, P.O. Box 513, 5600 MB Eindhoven, The Netherlands.

ABSTRACT One of the main features of any lithography technique is its resolution, generally maximized for a single isolated object. However, in most cases, functional devices call for highly dense arrays of nanostructures, the fabrication of which is generally challenging. Here, we show the growth of arrays of densely packed isolated nanowires based on the use of focused beam induced deposition plus Ar^+ milling. The growth strategy presented herein allows the creation of films showing thickness modulation with periodicity determined by the beam scan pitch. The subsequent Ar^+ milling translates such modulation into an array of isolated nanowires. This approach has been applied to grow arrays of W-based nanowires by focused ion beam induced deposition and Co nanowires by focused electron beam induced deposition, achieving linear densities up to 2.5×10^7 nanowires/cm (one nanowire every 40 nm). These results open the route for specific applications in nanomagnetism, nanosuperconductivity, and nanophotonics, where arrays of densely packed isolated nanowires grown by focused beam deposition are required.

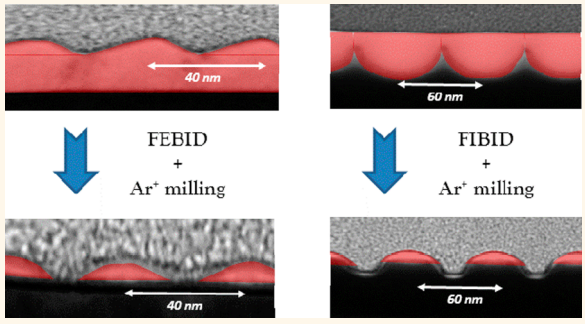

KEYWORDS: focused electron beam induced deposition · focused ion beam induced deposition · nanowires · nanolithography · transmission electron microscopy

Lithography involves a set of techniques that allow the patterning of materials and devices down to micro/nano dimensions, including integration and process parallelization.[1−3] One of the main attributes of any lithography technique is its resolution, which, generally speaking, indicates the minimum structure size achievable with such technique. Importantly, the resolution strongly depends on the geometrical shape of the structure. In general, the achievable resolution for a one-dimensional structure (nanowire) is worse compared to a zero-dimensional structure (dot) because the fabrication of a continuous and homogeneous one-dimensional structure is more challenging. A prominent example is the case of focused ion beam (FIB) patterning, where a resolution of 3 nm has been obtained in the patterning of a single hole in a membrane;[4] however, the resolution achieved in FIB patterning to obtain one single nanowire hardly reaches 10 nm.[5] Moreover, it is far more challenging to achieve high resolution in densely packed structures than in a single object, for example, in the fabrication of Fresnel zone plates by FIB, where the resolution is only 100 nm.[6,7] Similar discussions can be given for the different lithography techniques. For many real applications, densely packed high-resolution structures have to be achieved. Over the past decade, there has been a significant effort in the field of focused beam induced deposition to demonstrate that high resolutions (on the order of only a few nanometers) can be achieved, but until now, the functionality of the deposits at these small scales has received little attention. Our target is to explore novel routes to achieve densely packed structures based on functional materials grown by focused beam induced deposition.

* Address correspondence to deteresa@unizar.es.

Received for review January 26, 2014 and accepted March 19, 2014.

Published online March 19, 2014
10.1021/nn500525k

Focused ion beam induced deposition (FIBID) and its sister technique focused electron beam induced deposition (FEBID) are single-step lithography techniques where a precursor is provided to the area of interest by means of a gas injection system.[8−12] A deposit grows in the scanning area and contains one or more chemical elements from the precursor. As a first approximation, the grown deposit shows the same geometrical shape of the beam scanning (dot, line, square, arbitrary, and so forth). Nowadays, one can find plenty of applications where focused beam induced deposition is used: circuit editing and mask repair,[13] lamella protection,[14] nanoprototyping,[15] gas sensing,[16] nano-optics,[17] nanomagnetism,[18] superconductivity,[19] strain sensing,[20] *etc.* So far, great effort has been put toward improving the resolution of this technique. In the case of an isolated single dot or single line, the resolution in dedicated experiments can be very high, in the realm of one or a few nanometers.[21−23] However, the growth of closely spaced structures brings about the growth of a relatively thick base layer caused by the precursor dissociation beyond the incident beam spot.[21−26] This effect is inherent to the technique and mainly caused by the secondary electrons produced when the primary beam impacts the substrate or the growing structures.[27] As a result, instead of an array of densely packed isolated nanowires, the sample should be considered a continuous film with thickness modulation (corrugation). This can be a problem in certain applications where the functional properties are obtained only if these nanowires are isolated from each other. For instance, W-based superconducting nanowires grown by FIBID show remarkable finite-size effects due to the existence of a surface barrier,[28] which would be lost in an array of nanowires connected by the base. Another example is the case of arrays of Co or Fe ferromagnetic nanowires grown by FEBID, where the magnetic properties are very sensitive to a background or halo layer.[26,29−31]

In the present work, we propose a two-step process to obtain arrays of densely packed isolated nanowires by FEBID or FIBID. First, thickness modulation is achieved using small beam scan pitch in the direction perpendicular to the nanowires. Such pitch value determines the nanowire center-to-center distance; however, this produces a connecting base layer among the nanowires. In the second step, a soft Ar^+ milling eliminates such base layer, producing an array of densely packed isolated nanowires. Hereafter, this approach is applied to grow arrays of isolated W-based nanowires by FIBID and Co nanowires by FEBID, achieving linear densities up to 2.5×10^7 nanowires/cm (one isolated nanowire every 40 nm).

RESULTS AND DISCUSSION

Description of the Nanofabrication Method. The approach presented here consists of two steps and is sketched in Figure 1. In the first step, thickness-modulated deposits

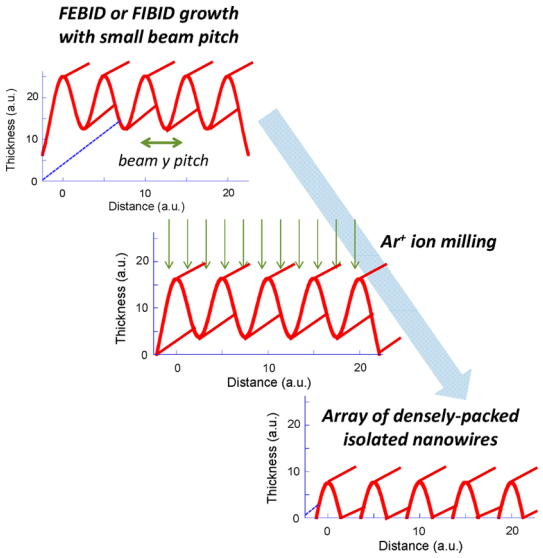

Figure 1. Sketch showing the steps followed to achieve the growth of arrays of densely packed nanowires: first, the growth of the arrays by FEBID or FIBID with controlled small beam pitch; second, the Ar^+ milling step.

are grown by FEBID or FIBID. The thickness modulation is achieved with a serpentine scan strategy, where the beam scans a line (*x* direction) from left to right, then moves to the next line and scans a line from right to left, then moves to the next line and scans from left to right. The movement along the lines is controlled *via* the *x* pitch (the distance between two addressing points in the line) and the dwell time (the time that the beam stays fixed on the addressing point). The *y* pitch determines the distance between two consecutive lines. However, when a large number of structures are targeted in a small area, this gives rise to a connecting base layer, impeding the physical isolation of the individual structures. In the nanofabrication method of nanowire arrays proposed here, the growth parameters should be chosen in such a way that the thickness modulation provided by the *y* pitch survives. In such a case, the connecting base layer will be a background layer that can be eliminated by Ar^+ milling, which is the second step of the process. Ar^+ milling is known to be a soft milling process capable of reliably transferring patterns in metals, in particular, cobalt.[32] The final resolution of this nanofabrication method can be limited by different physical effects occurring during ion milling.[33] In the present work, we show that isolated nanowires with a periodicity of 40 nm can be readily achieved. With further optimization in both steps (sample growth and Ar^+ ion milling), it is highly likely that this resolution can be improved.

Fabrication of Densely Packed Cobalt Nanowire Arrays by FEBID Plus Ar^+ Milling. Using the $Co_2(CO)_8$ precursor and the FEBID technique, cobalt functional deposits have been grown in the past.[34−36] We have even achieved the fabrication of single cobalt nanowires with a width of 30 nm, showing good magnetic properties.[37]

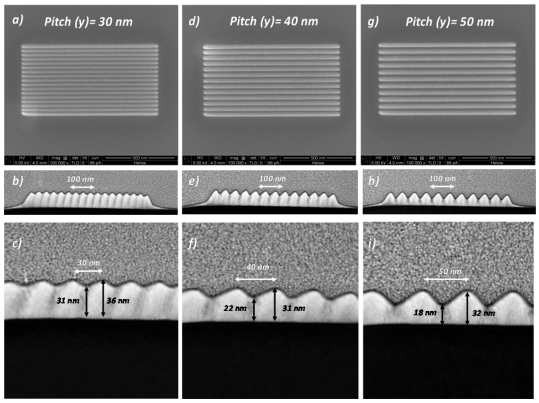

Figure 2. SEM (a,d,g) and HAADF-STEM (b,c,e,f,h,i) images of three arrays of cobalt FEBID nanowires grown with a pitch of 30 nm (a−c), 40 nm (d−f), and 50 nm (g−i).

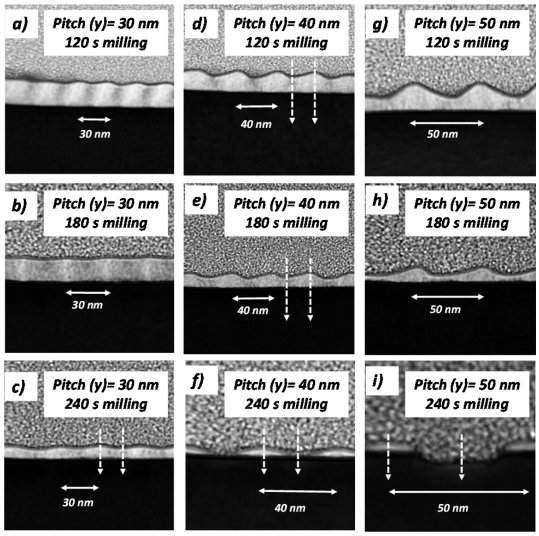

Figure 3. HAADF-STEM images of three arrays of cobalt FEBID nanowires grown with a pitch of 30 nm (a−c), 40 nm (d−f), and 50 nm (g−i) and Ar^+ milled during 120 s (a,d,g), 180 s (b,e,h), and 240 s (c,f,i). The trajectories of the EDS line scans shown in Figure 4 have been marked with white arrows.

We have applied the method described in the previous section using a *y* pitch of 30, 40, and 50 nm to explore how far we could successfully apply the method. Figure 2a,d,g shows the scanning electron microscopy (SEM) images of the three types of arrays. These top-down images of the arrays present clear contrast associated with the *y* pitch value used in each case. From such SEM images, it is impossible to conclude if the nanowires are connected through a base layer or are isolated. This information can be drawn from the scanning transmission electron microscopy (STEM) images shown in Figure 2b,c,e,f,h,i. In the high-angle annular dark-field (HAADF)-STEM images, the cobalt deposit shows a strong white contrast with respect to the Si substrate due to the higher atomic number of Co (27 *versus* 14). The three arrays display the same two features: thickness modulation with the same periodicity of the *y* pitch and the existence of a connecting base layer. A strong difference among the three arrays is the thickness of the connecting layer. Whereas the thickness of the base layer is 56% of the maximum thickness for the array with *y* pitch of 50 nm, it is 71% for the array with *y* pitch of 40 nm and 86% for the array with *y* pitch of 30 nm. As expected, this indicates that the transfer of the thickness modulation into isolated nanowires will be more difficult as the *y* pitch decreases. Next to the last nanowires of the arrays, the typical halo of an isolated structure is evident, which decays strongly with distance. Inside the array, the connecting base layer can be considered to be the addition of the halo produced during the growth of nearby nanowires, thus being much thicker.

Once the first step (thickness modulation) has been achieved, the second step (Ar^+ milling) is carried out. Given the thickness of the base layer in the three arrays (18, 22, and 31 nm, respectively) and when the milling rate of cobalt (6 nm/min) is taken into account, an easy calculation indicates that at least about 3 min would be required to completely mill the base layer of the 50 nm pitch sample and almost 4 min for the 40 nm pitch sample. As a consequence, on three identical samples, we performed milling for 120, 180, and 240 s, respectively, allowing us to image the progress of the milling process toward the nanowire isolation. STEM and energy-dispersive X-ray spectroscopy (EDS) experiments were subsequently carried out on lamellae prepared after the milling step. The corresponding STEM images are shown in Figure 3. It is observed that after 120 s (a,d,g) and 180 s (b,e,h) milling, both the maximum thickness and the connecting base layer have decreased in thickness, but the nanowire isolation has failed. After 240 s (c,f,i), the STEM images seem to indicate that the nanowire isolation is effectively produced in the arrays with *y* pitch of 40 and 50 nm. The nanowire physical separation is evident in the 50 nm pitch sample due to the noticeable etching of the substrate. The EDS line scan experiments are useful to be conclusive on such physical isolation. Representative results are shown in Figure 4. Figure 4a represents (for the unmilled, 120 s milled, 180 s milled, and 240 s milled sample with 40 nm *y* pitch) the Co signal in line scans taken top-down from above the maximum thickness of the deposits toward the substrate. An informative drawing of the line scan position is indicated by means of white arrows in the images of Figure 3. From Figure 4a, it is possible to extract the information that the maximum thickness of the deposit decreases with the milling from 27 ± 2 nm (as-grown sample) to 18 ± 2 nm (120 s milling), 12 ± 2 nm (180 s milling), and 6 ± 2 nm (240 s milling). According to Figure 2f, when the difference between the maximum thickness and the base layer was about 9 nm for the unmilled sample, the soft Ar^+ milling process permitted an acceptable transfer of such thickness

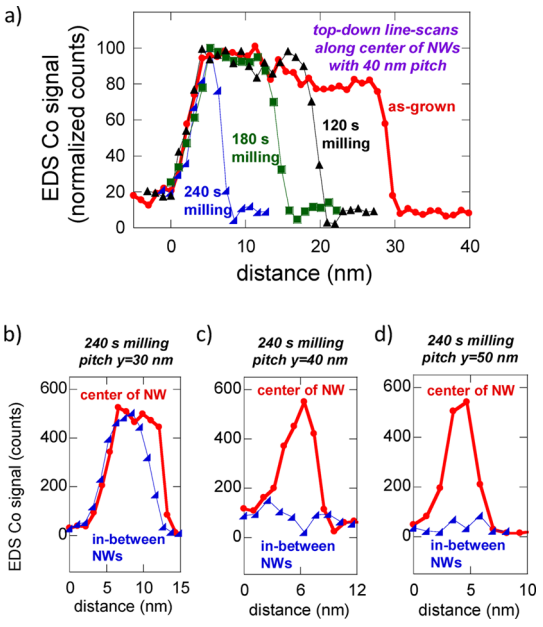

Figure 4. EDS measurements in the arrays of cobalt FEBID nanowires. (a) Comparison of the EDS cobalt signal in the 40 nm pitch nanowire array along lines from the top part of the nanowire down to the substrate (see white arrows in Figure 3) for the as-grown sample and after milling for 120, 180, and 240 s. (b) For the samples milled for 240 s (30, 40, and 50 nm pitch), comparison of the EDS cobalt signal in top-down line scans acquired at the center of the nanowire in comparison with those taken between the nanowires, showing the effective isolation of the nanowires only for a pitch of 40 and 50 nm.

modulation into isolated nanowires with a height of 6 ± 2 nm and a width about 30 nm according to Figure 3f. This means that the physical distance between neighboring nanowires is about 10 nm. For the sample with 50 nm pitch, after 240 s milling, the height of the nanowires is 5 ± 2 nm and the width is about 20 nm according to Figure 3i, meaning that the physical distance between neighboring nanowires is about 30 nm. For the sample with 30 nm pitch, the thickness modulation for the unmilled sample was only 5 nm. According to Figure 3c, nanowire isolation is not achieved in this sample after 240 s milling. It should be noted that perhaps further milling time could achieve the nanowire isolation in this sample, but in this case, the nanowire height would be too small for functional applicability.

EDS line scans were carried out from the center (thickest part) of the deposit, top-down toward the substrate as well as between the nanowires (the thinnest part), top-down toward the substrate (see the white arrows in Figure 3). This experiment is useful for checking the effective nanowire isolation in the sample milled for 240 s, as shown in Figure 4b–d. In this figure, we compare the cobalt signal in both cases. For the sample with 30 nm pitch, the cobalt signal is similar in number of counts between the nanowires and at the center of the nanowires, confirming the absence of physical isolation between the nanowires.

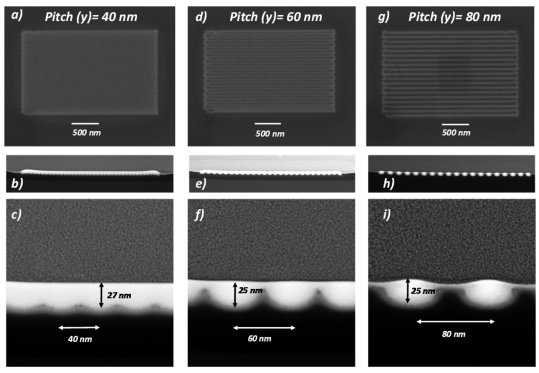

Figure 5. SEM (a,d,g) and HAADF-STEM (b,c,e,f,h,i) images of three arrays of W-based FIBID nanowires grown with pitch of 40 nm (a–c), 60 nm (d–f), and 80 nm (g–i).

However, in the case of the samples with 40 and 50 nm pitch, the cobalt signal between the nanowires is within the background signal, confirming the physical isolation of the nanowires.

In the Supporting Information, some further information about these cobalt arrays has been included for completeness. More specifically, the reader can find information about the EDS experiments in the as-grown sample, atomic force microscopy (AFM) measurements of the sample milled for 240 s, and MFM measurements in the sample milled for 120 s. The MFM experiments, which capture the magnetism of nanostructures, confirm that the soft Ar^+ milling step conserves the magnetism of the cobalt arrays.

Fabrication of Densely Packed W-Based Nanowires by FIBID Plus Ar^+ Milling. Given the relatively larger Ga^+ beam spot size on the sample surface at the selected current, 20 nm, we targeted maximum packing of one nanowire every 40 nm. The SEM images of the three types of W-based arrays grown, with *y* pitch of 40, 60, and 80 nm, are shown in Figure 5a,d,g. These SEM images suggest thickness modulation in the 60 and 80 nm pitch arrays but not in the 40 nm pitch sample. However, the HAADF-STEM images shown in Figure 5b,c,e,f, h,i show strong differences in the topography compared to the cobalt FEBID deposits discussed in the previous section. The substrate is effectively milled by the Ga^+ beam in the scanned areas, and the deposit mainly grows inside such drilled areas but also between them, given the precursor dissociation beyond the scanned areas. The effect is more pronounced as the *y* pitch value increases. For the particular conditions of our experiment, the Ga^+ milling rate of the Si substrate must be similar to the W-based deposit growth rate, producing deposits with apparent low thickness with respect to the substrate. This brings about a very small thickness modulation on the top surface but a significant modulation at the bottom one. Thus, the 40 nm pitch sample shown in Figure 5c displays an apparent flat top surface, whereas the thickness modulation is indeed present at the

bottom surface. For the 60 and 80 nm pitch samples, shown in Figure 5f,i, the thickness modulation is small at the top surface but is quite large at the bottom surface. Another difference with respect to the cobalt FEBID arrays is seen upon careful inspection of the SEM images in Figure 5a,d,g. In this case, the serpentine scan mode produces observable growth of deposit at the turning points of the ion beam. This is caused by the high efficiency of the Ga^+ ion beam in precursor dissociation, as shown by the short dwell times required here, 200 ns, compared with 20 μs in the case of cobalt deposits discussed previously. This effect in combination with a relatively slow motion of the ion beam at the turning points during serpentine scan mode would explain the observed behavior. If such deposit growth at the edges is an issue for some particular application of the arrays, it could be avoided in different ways such as using raster scan mode instead of serpentine scan, fast ion beam blanking at the end of each line, subsequent etching of the array edges, *etc*.

As shown in the Supporting Information, the EDS experiments indicate that the white contrast in the images corresponds to the W-based deposit, whereas the gray contrast below corresponds to the region without W but containing implanted Ga.

The three Ar^+ milling times used (60, 150, and 210 s) were chosen taking into account the calibrated milling rate of the W-based deposits (3 nm/min). As shown in Figure 6a,d,g, the deposits become thinner after 60 s Ar^+ milling, but the nanowire isolation is not achieved. As can be observed in Figure 6b,e,h, after 150 s milling, when the deposit thickness is about 10 nm, the nanowires from the array with a *y* pitch of 80 nm are isolated and those from the array with a *y* pitch of 60 nm are isolated or on the verge of being isolated. The array with a *y* pitch of 40 nm still presents the connecting base layer. The geometry of the isolated nanowires with y pitch of 80 nm is interesting, as can be observed in Figure 6h. Given the higher milling rate of the silicon substrate compared to that of the W-based deposit, the sample develops a strong peak–valley topography, where the isolated nanowires remain on the peaks. With further milling, using 210 s, such peak–valley topography is reinforced because the W deposit is acting as a "hard masking layer" with respect to the substrate due to the difference in the milling rates. Regarding the nanowire isolation, now the array with 60 nm *y* pitch shows well-separated nanowires, with dimensions of 30 nm in width at the base and thickness of 6 ± 2 nm. For the array with a *y* pitch of 40 nm, the STEM images are not very clear about the nanowire isolation.

From the EDS line scans displayed in Figure 7a, information on the evolution of the maximum thickness of the 60 nm pitch sample with the milling can be obtained. It changes from 25 ± 2 nm (as-grown sample) to 22 ± 2 nm (60 s milling), 15 ± 2 nm (150 s milling), and 6 ± 2 nm (210 s milling). This indicates a tendency to increase the milling rate as the thickness of the deposit decreases.

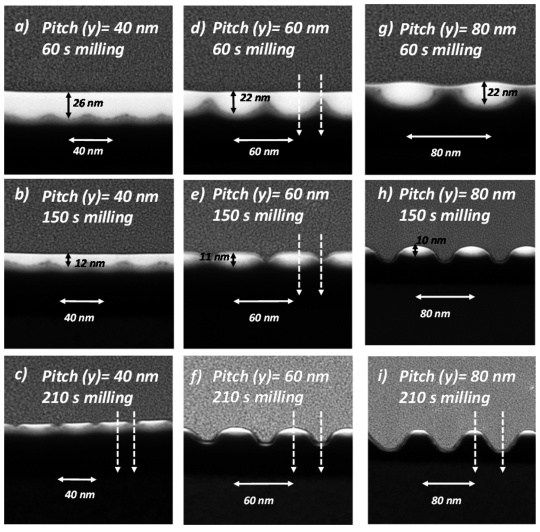

Figure 6. HAADF-STEM images of three arrays of W-based FIBID nanowires grown with pitch of 40 nm (a–c), 60 nm (d–f), and 80 nm (g–i) and Ar^+ milled during 60 s (a,d,g), 150 s (b,e,h), and 210 s (c,f,i). The trajectories of the EDS line scans shown in Figure 7 have been marked with white arrows.

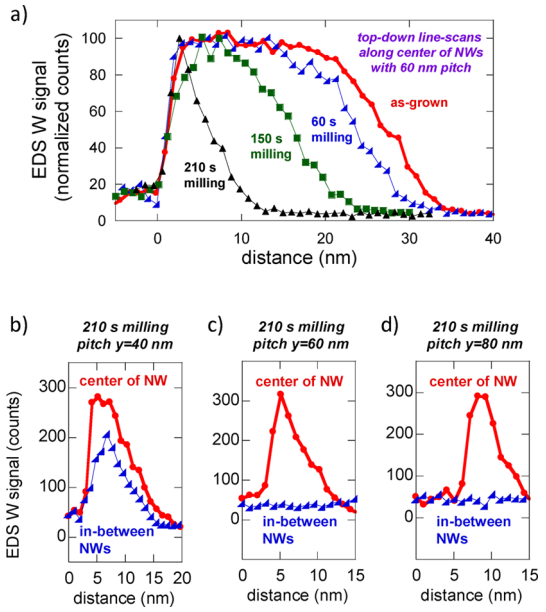

Figure 7. EDX line scans of the array of W-based FIBID nanowires grown with a pitch of 60 nm. (a) Comparison of the W signal along lines from the top of the nanowire down to the substrate (see white arrows in Figure 6) for the as-grown sample and the samples milled for 60, 150, and 210 s, respectively. (b) For the 40 nm pitch sample milled for 210 s, comparison of the W signal in a line scan taken in the center of the nanowire with a line scan taken between the nanowires. (c) Same for the 60 nm pitch sample. (d) Same for the 80 nm pitch sample.

The nanowire isolation in the arrays with a *y* pitch of 60 and 80 nm can be deduced from the EDS line scans shown in Figure 7b–d. The W signal disappears between the nanowires for the samples with a *y* pitch of 60 and 80 nm but is present for the array with a 40 nm pitch. However, the number of counts is lower between the nanowires compared to the center of the nanowires, suggesting less W content. One could speculate that such composition difference could give rise to higher conductive paths separated by less conductive separation regions, which could still show the searched functionality for the isolated nanowires.

In the present work, we have achieved the nanofabrication of arrays of cobalt FEBID nanowires separated by 40 nm (center-to-center) and W-based FIBID nanowires separated by 60 nm. Using this approach, such good resolution in the packing of nanowires can definitely be improved in the future given the large number of parameters involved in FEBID and FIBID. By using lower beam currents, the beam spot size will decrease and smaller *y* pitch values could be used, decreasing the periodicity of the thickness modulation. In theory, there is significant margin for improvement considering that the lowest beam spot sizes currently achievable in SEM and FIB columns are about 1 and 3 nm, respectively. Another parameter that can be optimized is the deposit thickness because it is found that the thickness corrugation decreases as the deposit thickness increases. Concerning the Ar^+ milling step, *in situ* monitoring of the nanowire isolation could be useful to stop the milling in the very right moment. Such *in situ* monitoring during milling could be realized with secondary ion mass spectroscopy or electrical measurements. Additional discussion about the limitations of the present strategy can be found in the Supporting Information.

The method proposed here can be extrapolated to the fabrication of other densely packed isolated structures in addition to arrays of nanowires. The most natural ones are dots or pillars, but, in principle, any structure with arbitrary shape can be subjected to this method. This method is general for focused beam deposition techniques and can be applied to all functional materials grown by such techniques. Consequently, we anticipate relevant applications in the fields of nanomagnetism, nanophotonics, and nanosuperconductivity, where miniaturization and size effects in isolated single structures have already been shown to be of great importance.[17,28,29] More specifically, highly dense isolated nanostructures grown by focused beam deposition techniques can be envisaged and could find applications in magnetic storage and logic, in several types of miniaturized sensors, in superconducting vortex-based devices, *etc*.

CONCLUSIONS

In this article, a nanofabrication method to create functional densely packed arrays of isolated nanowires is presented. The method is based on the use of focused beam induced deposition techniques to grow thickness-modulated deposits with short periodicity plus a subsequent Ar^+ milling step. To demonstrate the feasibility of the method, two functional materials grown by focused beam have been chosen: a magnetic one and a superconducting one. First, arrays of isolated cobalt nanowires have been produced with a pitch of 40 and 50 nm. Second, arrays of isolated W-based nanowires have been produced with a pitch of 60 and 80 nm. These results constitute the basis for the design of functional (magnetic, superconducting, photonic, semiconducting, *etc*.) dense structures grown by focused beam showing particular applications or novel effects only achievable after the physical isolation of the individual structures.

EXPERIMENTAL SECTION

Growth of the Co-Based Arrays. The growth was carried out in a dual beam Helios 600 by FEI. A $Co_2(CO)_8$ precursor heated to 27 °C and a silicon wafer substrate were used. The injector needle tip was located 50 μm away in the *x*–*y* direction and 150 μm away in the *z* direction of the substrate surface. The chamber base pressure was 1×10^{-6} mbar, and the process pressure was 2.6×10^{-5} mbar. The electron beam was scanned in serpentine mode to grow arrays of nanowires in an area of 1 μm × 0.5 μm. The following parameters were used: beam voltage, 3 kV; beam current, 43 pA; dwell time, 20 μs; refresh time, 50 ms. Under such beam current, the estimated size of the electron beam spot on the sample surface was 10 nm. The beam pitches in the *y* direction (perpendicular to the nanowires) were chosen to be 30, 40, and 50 nm, respectively, for the three types of samples grown. The beam pitch in the *x* direction (along the nanowires) was chosen to be 4.74 nm in all cases. The total beam irradiation time was chosen to provide samples with a thickness of about 25 nm. As an example, the sample with a 30 nm *y* pitch was grown in 132 s. In order to check the appropriate deposit thickness modulation, SEM images were taken in some of the arrays using the through-lens detector (TLD) of the electron column in the Helios 600.

Growth of the W-Based Arrays. The growth was carried out in a dual beam Helios 600 by FEI. A $W(CO)_6$ precursor heated to 55 °C and a silicon wafer substrate were used. The injector needle tip was located 50 μm away in the *x*–*y* direction and 150 μm away in the *z* direction of the substrate surface. The chamber base pressure was 1×10^{-6} mbar, and the process pressure was 6×10^{-6} mbar. The Ga^+ beam was scanned in serpentine mode to grow arrays of nanowires in an area of 2.5 μm × 1.5 μm. The following parameters were used: beam voltage, 30 kV; beam current, 9.7 pA; dwell time, 200 ns. Under such beam current, the estimated size of the electron beam spot on the sample surface was 20 nm. The beam pitches in the *y* direction (perpendicular to the nanowires) were chosen to be 40, 60, and 80 nm, respectively, for the three types of samples grown. The beam pitch in the *x* direction (along the nanowires) was chosen to be 80 nm in all cases. The total beam irradiation time was chosen to provide samples with a thickness around 25 nm. As an example, the sample with a 40 nm *y* pitch was grown in 14 s. When needed, SEM images of the arrays were taken with the TLD detector using the Helios 600.

Ar^+ Milling Step. An ion milling system by Sistec was used. The chamber base pressure was below 1×10^{-6} mbar, and the process pressure was 4×10^{-4} mbar. The Ar plasma was created at the top part of the chamber and extracted and accelerated toward the sample by a grid held at 250 V negative voltage. About 12 sccm Ar gas was inserted in the top part of the chamber to create the plasma, and 3 sccm Ar gas was used in the neutralizer middle position. The neutralizer (a heated W filament) emitted controllable electron currents to avoid charging effects in the sample. The Ar^+ beam current was 90 mA, producing an Ar^+ dose of 0.5 mC/cm^2 s at the sample position. The milling rate of a sputtered cobalt thin film was previously calibrated to be 6 nm/min, and a similar rate was found in the Co deposits. The milling rate of the W deposits was found to be 3 nm/min.

TEM and EDS Characterization. The Helios 600 dual beam equipment was used to prepare thin lamellae of the arrays of nanowires in order to subsequently obtain high-resolution cross-sectional images by means of STEM. A Tecnai F30 by FEI was used for the STEM and EDS experiments. The equipment was operated at 300 kV in STEM mode: a small probe (less than 1 nm in diameter) was formed, and the sample was scanned pixel by pixel, acquiring the STEM images or the EDS spectra. The HAADF images taken in STEM mode had a strong element contrast, allowing the straightforward evaluation of the sample layers thickness. The EDS spectra were taken by scanning the electron beam, typically every 1 nm. The signal was collected by an EDAX detector integrated in the F30 equipment, presenting characteristic emission lines for the different elements. Specifically, the following emission lines were tracked in the EDS experiments: C (K edge), Co (K and L edges), O (K edge), Si (K edge), Ga (K and L edges), W (L edges). When comparison among different samples is carried out, the EDS counts were normalized due to the unknown lamellae thickness and other possible effects.

AFM Characterization. Commercial VEECO TMC Nanoscope V AFM equipment was used to characterize the topography of some of the nanowire arrays, especially during the optimization part of the work. Some of the cobalt nanowire arrays were measured in noncontact mode using a magnetic tip in order to check the existence of magnetic contrast.

Conflict of Interest: The authors declare no competing financial interest.

Acknowledgment. This work was supported by Spanish Ministry of Economy and Competitivity through Project No. MAT2011-27553-C02, including FEDER funds and by the Aragon Regional Government. Experimental help in the Ar milling experiments by R. Valero, in the TEM experiments by R. Fernández-Pacheco, and in the AFM/MFM experiments by J.L. Díez are warmly acknowledged. Manuscript reading by Scott Mitchell is acknowledged.

Supporting Information Available: Additional information is provided in a supplementary file. This material is available free of charge *via* the Internet at http://pubs.acs.org.

REFERENCES AND NOTES

1. Xia, Y. N.; Rogers, J. A.; Paul, K. E.; Whitesides, J. M. Unconventional Methods for Fabricating and Patterning Nanostructures. *Chem. Rev.* **1999**, *99*, 1823–1848.
2. Martín, J. I.; Nogues, J.; Liu, K.; Vicent, J. L.; Schuller, I. K. Ordered Magnetic Nanostructures: Fabrication and Properties. *J. Magn. Magn. Mater.* **2003**, *256*, 449–501.
3. Levinson, H. J. *Principles of Lithography*, 3rd ed.: SPIE Press: Bellingham, WA, 2010; eISBN: 9780819483256; print ISBN13: 9780819483249.
4. Schiedt, B.; Auvray, L.; Bacri, L.; Oukhaled, G.; Madouri, A.; Bourhis, E.; Patriarche, G.; Pelta, J.; Jede, R.; Gierak, J. Direct FIB Fabrication and Integration of "Single Nanopore Devices" for the Manipulation of Macromolecules. *Microelectron. Eng.* **2010**, *87*, 1300–1303.
5. Lucot, D.; Gierak, J.; Ouerghi, A.; Bourhis, E.; Faini, G.; Mailly, D. Deposition and FIB Direct Patterning of Nanowires and Nanorings into Suspended Sheets of Graphene. *Microelectron. Eng.* **2009**, *86*, 882–884.
6. Surpi, A.; Valizadeh, S.; Leifer, K.; Lagomarsino, S. Focused Ion Beam Fabrication Procedures of X-ray Micro Fresnel Zone Plates. *J. Micromech. Microeng.* **2007**, *17*, 617–622.
7. Nadzeyka, A.; Peto, L.; Bauerdick, S.; Mayer, M.; Keskinbora, K.; Grévent, C.; Weigand, M.; Hirscher, M.; Schütz, G. Ion Beam Lithography for Direct Patterning of High Accuracy Large Area X-ray Elements in Gold on Membranes. *Microelectron. Eng.* **2012**, *98*, 198–201.
8. Randolph, S. J.; Fowlkes, J. D.; Rack, P. D. Focused Nanoscale Electron-Beam-Induced Deposition and Etching. *Crit. Rev. Solid State Mater. Sci.* **2006**, *31*, 55–89.
9. Van Dorp, W. F.; Hagen, C. W. A Critical Literature Review of Focused Electron Beam Induced Deposition. *J. Appl. Phys.* **2008**, *104*, 081301.
10. Utke, I.; Hoffmann, P.; Melngailis, J. Gas Assisted Focused Electron and Ion Beam Processing and Fabrication. *J. Sci. Vac. Technol., B* **2008**, *26*, 1197–1276.
11. Russell, P. E.; Utke, I.; Moshkalev, S., Eds. *Nanofabrication Using Focused Ion and Electron Beams: Principles and Applications*; Oxford University Press: New York, 2012; ISBN: 9780199734214.
12. Huth, M.; Porrati, F.; Schwalb, C.; Winhold, M.; Sachser, R.; Dukic, M.; Adams, J.; Fantner, G. Focused Electron Beam Induced Deposition: A Perspective. *Beilstein J. Nanotechnol.* **2012**, *3*, 597–619.
13. Stewart, D. K.; Stern, L. A.; Morgan, J. C. Focused-Ion-Beam Induced Deposition of Metal for Microcircuit Modification. *SPIE Proc.* **1989**, *1089*, 18.
14. Gianuzzi, L. A.; Stevie, F. A. *Introduction to Focused Ion Beams*; Springer Science: Boston, MA, 2005.
15. Reyntjens, S.; Puers, R. A Review of Focused Ion Beam Applications in Microsystem Technology. *J. Micromech. Microeng.* **2001**, *11*, 287–300.
16. Hernández-Ramírez, F.; Tarancón, A.; Casals, O.; Rodríguez, J.; Romano-Rodríguez, A.; Morante, J. R.; Barth, S.; Mathur, S.; Choi, T. Y.; Poulikakos, D.; *et al.* Fabrication and Electrical Characterization of Circuits Based on Individual Tin Oxide Nanowires. *Nanotechnology* **2006**, *17*, 5577–5583.
17. Weber-Bargioni, A.; Schwartzberg, A.; Schmidt, M.; Harteneck, B.; Ogletree, D. F.; Schuck, P. J.; Cabrini, S. Functional Plasmonic Antenna Scanning Probes Fabricated by Induced-Deposition Mask Lithography. *Nanotechnology* **2010**, *21*, 065306.
18. Fernández-Pacheco, A.; Serrano-Ramón, L.; Michalik, J.; Ibarra, M. R.; De Teresa, J. M.; O'Brien, L.; Petit, D.; Lee, J.; Cowburn, R. P. Three Dimensional Magnetic Nanowires Grown by Focused Electron-Beam Induced Deposition. *Sci. Rep.* **2013**, *3*, 1492.
19. Sadki, E. S.; Ooi, S.; Hirata, K. Focused-Ion-Beam-Induced Deposition of Superconducting Nanowires. *Appl. Phys. Lett.* **2004**, *85*, 6206–6208.
20. Schwalb, C. H.; Grimm, C.; Baranowski, M.; Sachser, R.; Porrati, F.; Reith, H.; Das, P.; Müller, J.; Völklein, F.; Kaya, A.; *et al.* A Tunable Strain Sensor Using Nanogranular Metals. *Sensors* **2010**, *10*, 9847–9856.
21. Van Dorp, W. F.; van Someren, B.; Hagen, C. W.; Kruit, P.; Crozier, P. A. Approaching the Resolution Limit of Nanometer-Scale Electron Beam-Induced Deposition. *Nano Lett.* **2005**, *5*, 1303–1307.
22. Van Kouwen, L.; Botman, A.; Hagen, C. W. Focused Electron-Beam-Induced Deposition of 3 nm Dots in a Scanning Electron Microscope. *Nano Lett.* **2009**, *9*, 2149–2152.
23. Van Oven, J. C.; Berwald, F.; Berggren, K. K.; Kruit, P.; Hagen, C. W. Electron-Beam-Induced Deposition of 3-nm-Half-Pitch Patterns on Bulk Si. *J. Sci. Vac. Technol., B* **2011**, *29*, 06F305.
24. Crozier, P. A. Proximity Effects in Nanoscale Patterning with High Resolution Electron Beam Induced Deposition. *J. Sci. Vac. Technol., B* **2008**, *26*, 249–254.
25. Plank, H.; Smith, D. A.; Haber, T.; Rack, P.; Hofer, F. Fundamental Proximity Effects in Focused Electron Beam Induced Deposition. *ACS Nano* **2012**, *6*, 286–294.

26. Nikulina, E.; Idigoras, O.; Porro, J. M.; Vavassori, P.; Chuvilin, A.; Berger, A. Origin and Control of Magnetic Exchange Coupling in between Focused Electron Beam Deposited Cobalt Nanostructures. *Appl. Phys. Lett.* **2013**, *103*, 123112.
27. Van Dorp, W. F.; Beyer, A.; Mainka, M.; Gölzhäuser, A.; Hansen, T. W.; Wagner, J. B.; Hagen, C. W.; De Hosson, J. T. Focused Electron Beam Induced Processing and the Effect of Substrate Thickness Revisited. *Nanotechnology* **2013**, *24*, 345301.
28. Córdoba, R.; Baturina, T. I.; Sesé, J.; Mironov, A. Y.; De Teresa, J. M.; Ibarra, M. R.; Nasimov, D. A.; Gutakovskii, A. K.; Latyshev, A. V.; Guillamón, I.; *et al.* Magnetic Field Induced Dissipation Free State in Superconducting Nanostructures. *Nat. Commun.* **2013**, *4*, 1437.
29. Fernández-Pacheco, A.; De Teresa, J. M.; Szkudlarek, A.; Córdoba, R.; Ibarra, M. R.; Petit, D.; Read, D. E.; O'Brien, L.; Lewis, E. R.; Zeng, H. T.; *et al.* Magnetization Reversal in Individual Cobalt Micro- and Nano-wires Grown by Focused-Electron-Beam-Induced-Deposition. *Nanotechnology* **2009**, *20*, 475704.
30. Serrano-Ramón, L.; Fernández-Pacheco, A.; Córdoba, R.; Magén, C.; Rodríguez, L. A.; Petit, D.; Cowburn, R. P.; Ibarra, M. R.; De Teresa, J. M. Improvement of Domain Wall Conduit Properties in Cobalt Nanowires by Global Gallium Irradiation. *Nanotechnology* **2013**, *24*, 345703.
31. Gavagnin, M.; Wanzenboeck, H. D.; Belic, D.; Shawraw, M. M.; Persson, A.; Gunnarsson, K.; Svedlindh, P.; Bertagnolli, E. Magnetic Force Microscopy Study of Shape Engineered FEBID Iron Nanostructures. *Phys. Status Solidi A* **2013**, *211*, 368–374.
32. Moneck, M. T.; Zhu, J. G.; Che, X. D.; Tang, Y. S.; Lee, H. J.; Zhang, S. Y.; Moon, K. S.; Takahashi, N. Fabrication of Flyable Perpendicular Discrete Track Media. *IEEE Trans. Magn.* **2007**, *43*, 2127–2129.
33. Li, K.-D. Modeling of Feature Profile Evolution for Ion Etching. *J. Appl. Phys.* **2013**, *113*, 014305.
34. Utke, I.; Hoffmann, P.; Berger, R.; Scandella, L. High-Resolution Magnetic Co Supertips Grown by a Focused Electron Beam. *Appl. Phys. Lett.* **2002**, *80*, 4792–4794.
35. Boero, G.; Utke, I.; Bret, T.; Quack, N.; Todorova, M.; Mouaziz, S.; Kejik, P.; Brugger, J.; Popovic, R. S.; Hoffmann, P. Submicrometer Hall Devices Fabricated by Focused Electron-Beam-Induced Deposition. *Appl. Phys. Lett.* **2005**, *86*, 042503.
36. Fernández-Pacheco, A.; De Teresa, J. M.; Córdoba, R.; Ibarra, M. R.; Petit, D.; Read, D. E.; O'Brien, L.; Lewis, E. R.; Zeng, H. T.; Cowburn, R. P. Domain Wall Conduit Behaviour in Cobalt Nanowires Grown by Focused-Electron-Beam Induced Deposition. *Appl. Phys. Lett.* **2009**, *94*, 192509.
37. Serrano-Ramón, L.; Córdoba, R.; Rodríguez, L. A.; Magen, C.; Snoeck, E.; Gatel, C.; Serrano, I.; Ibarra, M. R.; De Teresa, J. M. Ultra-small Functional Ferromagnetic Nanostructures Grown by Focused-Electron-Beam-Induced Deposition. *ACS Nano* **2011**, *5*, 7781–7787.